Critical fluctuations in an optical parametric oscillator: when light behaves like magnetism

Kaled Dechoum[1], Laura Rosales-Zárate[2] and Peter D. Drummond[2]
(1) Instituto de Física da Universidade Federal Fluminense, Boa Viagem, 24210-340, Niterói, Rio de Janeiro, Brazil
(2) Centre for Quantum and Optical Science, Swinburne University of Technology, Melbourne, Australia.

We study the non-degenerate optical parametric oscillator in a planar interferometer near threshold, where critical phenomena are expected. These phenomena are associated with non-equilibrium quantum dynamics that are known to lead to quadrature entanglement and squeezing in the oscillator field modes. We obtain a universal form for the equation describing this system, which allows a comparison with other phase transitions. We find that the unsqueezed quadratures of this system correspond to a two-dimensional XY type model with a tricritical Lifshitz point. This leaves open the possibility of a controlled experimental investigation into this unusual class of statistical models. We evaluate the correlations of the unsqueezed quadrature using both an exact numerical simulation and a Gaussian approximation, and obtain an accurate numerical calculation of the non-Gaussian correlations.

I. INTRODUCTION

Non-equilibrium pattern-formation occurs in many physical systems, giving rise to the emergence of order on macroscopic scales [1]. The theory of hydrodynamics is a paradigm for understanding these phenomena, and is applicable to many branches of physics, chemistry, biology, astrophysics, and other sciences [2]. This is often applied to many body systems subject to nonlinear coupling in a dissipative environment with external fluxes. In physics, one of the most studied hydrodynamic effects is the theory of fluid flows near the Rayleigh-Bénard instability instability [1]. The simplest nontrivial model for fluid convection that displays pattern formation due to convective instabilities was derived by Swift and Hohenberg [3], where nonlinear coupling of fluctuations was included to demonstrate the failure of mean field theory for critical exponents.

Here, we treat pattern formation and universality in a paradigmatic non-equilibrium *quantum* system: the non-degenerate parametric oscillator (OPO). Theories of a similar nature have been applied to non-equilibrium spatially extended structures in lasers and other related systems, with an emphasis on universal behavior of phase-transitions, pattern formation and self-organization [4]. Yet down-conversion in a non-degenerate parametric system can display new possibilities not found in these simpler cases. In particular, one can have entanglement and EPR paradoxes [5, 6].

In the present paper, we investigate a new type of critical point phase transition in this non-equilibrium quantum system in order to understand the universality class. In a type II OPO, there are two down-converted fields with orthogonal polarization. Hence, the order parameter is a complex or vector field in two dimensions. The two components of this vector field are associated with the polarization degrees of freedom of the down-converted radiation field. This is a quantum system driven to a phase transition far from thermal equilibrium. It is also known to display strong quantum entanglement and EPR correlations [5] in the case where there are two correlated output modes. We wish to understand the behavior of this phase-transition using a first-principles analysis [7, 8] of the relevant master equation.

Experimentally, the OPO is now a mature technology with both commercial and fundamental applications. Following initial theoretical predictions [9, 10], the quantum limited type I OPO was investigated experimentally by Wu et al [11], demonstrating quantum squeezing. Later the type II case, in a triply resonant cavity, was used to experimentally demonstrate continuous variable EPR correlations [6], also originally predicted theoretically [7, 8]. These initial experimental investigations were in few mode devices. Both below and above threshold experiments have been carried out, as close as $\pm 1\%$ of the critical point [12–17], confirming predictions of thresholds and conversion efficiency. Operation at the critical point results in low-frequency critical fluctuations and non-Gaussian behavior [18].

Spatially extended pattern formation in a degenerate or type I OPO has also been analyzed previously [19]. It is related to the Lifshitz phase transition [20]. This is a model used to describe the phase transition to a modulated magnetic phase [21, 22]. In this simplest case one has a two dimensional, planar system with a scalar order parameter [23], which has known universality properties. A Swift Hohenberg equation was derived for spatially extended nondegenerate type I OPOs with flat end mirrors [24], but ignoring fluctuations. OPO experiments have been recently extended to these types of multi-mode devices [25, 26], with type II as well as type I parametric downconversion. The experimental situation is that while multimode experiments have mostly used confocal mirrors, the first type II multimode planar mirror experiments have been carried out [26].

Studies of the Swift Hohenberg equation in the neighborhood of the critical point, the Lifshitz point, as well as pattern formation for lasers have been discussed [27]. The Lifshitz point is similar to the tricritical point [28].

Tricritical points occur in different physical systems. They correspond to a point in a phase-diagram where two lines of ordinary critical points meet and terminate [29]. For critical points and tricritical points there are two critical dimensions. The *upper* critical dimension refers to the one above which the critical exponents have classical values [28]. The *lower* critical dimension refers to the smallest dimension for which there is a true phase-transition, due to increasing fluctuations as the dimension is decreased.

Systems like these can entangle large numbers of modes, with quantum entanglement increasing as threshold is approached. Currently, experiments near the critical point are sensitive to classical fluctuations [18] and heating effects [26]. With improved stabilization methods, we expect that these technical problems can be overcome. However, noise due to quantum fluctuation effects will remain.

Theoretically, the usual approach for two-dimensional non-equilibrium problems is the Landau-Ginzburg (LG) equation [30], which was first used for understanding superconductivity near threshold. Normally, the LG equation is derived using approximations like adiabatic elimination, and is taken as an effective equation for the physical system. There is now an increased interest in extended spatial and multi-mode structures [25, 31] in the quantum optical parametric oscillator (OPO) [11, 32], due to availability of multiple transverse mode cavities [33] and quantum imaging control [34]. It is important in these cases to understand how quantum noise enters the dynamical equations [35].

We show that planar type-II down-conversion creates a non-equilibrium system with a similar general type of symmetry to the Berezinskii [36] and Kosterlitz-Thouless (BKT) model [37], but with an isotropic Lifshitz point, first studied in magnetic systems by Hornreich et al [28]. Physically, this is not a classical fluid or magnetic system, but rather is a quantum system, driven into a non-equilibrium critical point [38] far from thermal equilibrium. The non-degenerate planar OPO is fundamentally different to the usual BKT model, having a quartic rather than quadratic momentum-dependence in the linear response function. This places it in a similar category to the Swift-Hohenberg model and next-nearest neighbor lattice models. Our model can also display strong EPR entanglement and other nonclassical properties in addition to the Lifshitz point behavior. The parametric model therefore provides a novel path to the investigation of unusual classical and quantum noise effects.

Phase transitions with this general type of symmetry are continuous yet break no symmetries. There is also no ferromagnetism in this system, as this is prohibited by the Mermin-Wagner theorem [39]. Berezinskii predicted a new type of phase with correlations that decay slowly with distance with a power law. The phase transition for a ferromagnetic phase is prevented by the appearance of vortex and anti-vortex pairs. Many quantum phase transitions in two dimensions belong to this class. The continuous version of the XY or Ising models are often used to model systems that possess order parameters with a symmetry of this type, e.g. superfluid helium, liquid crystals, two dimensional Bose Einstein condensate (BEC), and others. While having the same order-parameter and space dimension as this case, we show that the type II OPO has a different universality class.

Our approach is to start from the usual master equation model that describes a type II OPO with transverse modes. Here we consider that the OPO is non-degenerate in polarization. We then map the coupled Heisenberg equations into the positive P-representation [40] of the density matrix. This choice is made because the positive P-representation allows us to *exactly* map the density matrix evolution into an equivalent stochastic equation.

We organize this paper in the following way. First we describe the Hamiltonian model and derive the equation of motion for this open system. Next, we use the positive-P representation for mapping these equation into a Langevin type, which can either be treated numerically or via analytic approximations. We will mostly describe the unsqueezed quadratures of the field, which have a large similarity with the corresponding magnetic system. At this point we can recognize the universality class. We give both a Gaussian approximation to the correlation functions of the unsqueezed quadratures, and high-precision numerical simulations of the non-Gaussian corrections. We show that, even though the system is far below its upper critical dimension, the non-Gaussian character of the fluctuations is relatively small, and the intensity fluctuations are nearly factorizable.

In a following paper we will focus our attention on the squeezed field quadratures, to give a spatial map of quantum squeezing and Einstein-Podolsky-Rosen (EPR) entanglement.

II. THE MODEL

The system of interest comprises an optically driven planar Fabry-Perot cavity or interferometer with a nonlinear medium that possess a parametric nonlinearity. The nonlinear crystal is cut to give a type II phase matching, that couples a pump field to two down-converted fields having an orthogonal polarization. The cavity is pumped with a spatially extended coherent light with frequency ω_0, with a transverse spatial profile. In the simplest case we consider this pump to be a plane wave.

A. Quantum Hamiltonian

The outgoing down-converted light, amplified inside the cavity, develops structures and patterns due to diffraction, nonlinear coupling, and detuning between the wavelength of the down-converted field and the cavity size. This depends on the modal decomposition of this

cavity. The mirrors have parameters that can be controlled by experimentalists. The tunable parameters include the reflection coefficient for each mode, and the cavity detunings for each mode.

Our model for this system is similar to many earlier treatments of driven nonlinear optical cavities [7, 9, 31, 41–45]. It includes a linear coupling between the external electromagnetic field modes and the internal cavity modes, owing to a partially transmitting mirror. The cavity and mirror parameters determine both the coupling to the driving field and the decay rate of the cavity or interferometer. We note that for a low-Q device, it is important to use non-orthogonal quasi-modes [42]. Here, we assume the opposite case of a thin, high-Q extended planar cavity, so that the external modes are simply plane-wave modes.

The quantum Hamiltonian in the interaction picture has four main terms that can be summarized by the following expression:

$$\hat{H} = \hat{H}_{free} + \hat{H}_{int} + \hat{H}_{pump} + \hat{H}_{res}\,, \tag{2.1}$$

where there are three fundamental Bose fields, $\hat{A}_i(\boldsymbol{x},t)$ for $i = 0, 2$. The boson fields are the transverse internal modes of the planar cavity, which is assumed to have a single longitudinal mode in the direction normal to the mirrors. We note that this planar polariton field model is also used in the theory of a polaritonic BEC [46]. The boson fields have two orthogonal polarizations, $i = 1, 2$, and obey the usual equal time commutation relation,

$$\left[\hat{A}_i(\boldsymbol{x},t), \hat{A}_j^\dagger(\boldsymbol{x}',t)\right] = \delta_{ij}\delta^2\left(\boldsymbol{x}-\boldsymbol{x}'\right).$$

Here $\delta^2\left(\boldsymbol{x}-\boldsymbol{x}'\right)$ is a Dirac delta function in the two-dimensional transverse plane of $\boldsymbol{x} = (x, y)$. The cavity fields are defined in terms of polaritonic annihilation and creation operators as: $\hat{A}_i(\boldsymbol{x},t) = \sum_{\boldsymbol{k}} e^{i\boldsymbol{k}\cdot\boldsymbol{x}}\hat{a}_i(\boldsymbol{k},t)/L$, where $\hat{a}_i(\boldsymbol{k},t)$ represents the annihilation operator for a free polariton mode with transverse momentum $\boldsymbol{k}$, and the summation is over a set of M discrete modes with periodic boundary conditions, on a large area L^2.

The free evolution Hamiltonian that accounts for diffraction inside the planar cavity is:

$$\hat{H}_{free} = \sum_{i=0}^{2}\hbar\int d^2\boldsymbol{x}\,\hat{A}_i^\dagger\left[\omega_i - \frac{v_i^2}{2\omega_i}\nabla^2\right]\hat{A}_i. \tag{2.2}$$

This Hamiltonian describes a planar cavity with intracavity resonant frequencies ω_i and group velocities v_i for the three field envelopes. The resonant frequencies have the relation $\omega_0 \approx \omega_1 + \omega_2$, where ω_0 is the fundamental mode, and ω_1 and ω_2 stand for the down-converted light. The case of spherical mirrors can also be analyzed in a similar way [33], but is not treated here. We suppress the field space-time arguments to obtain more compact expressions in the integrals. The two-dimensional Laplacian is, as usual, $\nabla^2 = \partial^2/\partial x^2 + \partial^2/\partial y^2$. A one-dimensional system can be treated by simply dropping one of the dimensions.

The interaction Hamiltonian representing the coupled modes inside a crystal with $\chi^{(2)}$ nonlinearity is given by [47]:

$$\hat{H}_{int} = i\hbar\int d^2\boldsymbol{x}\left[\chi\hat{A}_0\hat{A}_1^\dagger\hat{A}_2^\dagger - \chi^*\hat{A}_0^\dagger\hat{A}_1\hat{A}_2\right]. \tag{2.3}$$

This term may represent a photon of frequency ω_0 converted in two photons of distinct frequencies ω_1 and ω_2, or photons with orthogonal polarizations, or both.

From now on, for definiteness, labels 1 and 2 stand for polarizations, and we shall focus on the degenerate frequency case with non-degenerate polarization. For dimensional reasons, $\chi \propto \chi^{(2)}/\sqrt{\ell}$, where $\chi^{(2)}$ is the Bloembergen nonlinear polarizability coefficient and ℓ is the intracavity longitudinal mirror spacing.

Following standard input-output theory derivations [9, 10, 43–45], the Hamiltonian term associated with the input laser pumping in a rotating frame at frequency ω_L is:

$$\hat{H}_{pump} = i\hbar\int d^2\boldsymbol{x}\left[\mathcal{E}^*(\boldsymbol{x})e^{2i\omega_L t}\hat{A}_0 - \mathcal{E}(\boldsymbol{x})e^{-2i\omega_L t}\hat{A}_0^\dagger\right]. \tag{2.4}$$

While it is possible to choose any shape carrying spatial structure for the input pump, here for simplicity we will assume a plane wave input. The reservoir Hamiltonian is assumed to have the structure:

$$\hat{H}_{res} = \sum_{i=0}^{2}\int d^2\boldsymbol{x}\,\left[\hat{\Gamma}_j^\dagger\hat{A}_j + \hat{\Gamma}_j\hat{A}_j^\dagger\right] + \hat{H}_{res}^0\,. \tag{2.5}$$

Hence, there are local coupling terms to independent external free-field reservoirs for each polarization and each spatial mode. The external fields are described by a free Hamiltonian $\hat{H}_{res}^0$.

B. Master equation

The non-unitary evolution of the system comes from the coupling between the cavity modes and the output modes. This can be treated as a quantum Markovian process that simulates a bath interaction. We carry out this calculation in a type of interaction picture so that the interaction picture operators evolve according to a reference Hamiltonian $\hat{H}_0$, given by:

$$\hat{H}_0 = \hbar\sum_j\int d^2\boldsymbol{x}\,\omega_j^0\hat{A}_j^\dagger\hat{A}_j\,, \tag{2.6}$$

where the reference frequencies ω_1^0 are chosen so that:

$$\begin{aligned}\omega_1^0 &= \omega_L + \epsilon \approx \omega_1,\\ \omega_2^0 &= \omega_L - \epsilon \approx \omega_2,\\ \omega_0^0 &= 2\omega_L \approx \omega_0.\end{aligned} \tag{2.7}$$

We note that while the choice of ω_L is determined by the pump frequency, the choice of ϵ is arbitrary, as long as

the Markovian approximation is still valid. Our choice of reference Hamiltonian is not determined by the intracavity frequencies ω_i, which leads to detuning terms occurring in the resulting equations of motion. This allows us to have some freedom of choice in defining the detuning parameters. The choice will be made definite in the following sections. Following standard techniques for deriving the master equations [41, 43, 48], we can write the master equation for the density operator in the generalized Lindblad form:

$$\frac{\partial\hat{\rho}}{\partial t}=\frac{1}{i\hbar}\left[\hat{H},\hat{\rho}\right]+\sum_{i=0}^{2}\gamma_i\mathcal{L}_i\left[\hat{\rho}\right], \tag{2.8}$$

where the dissipative Liouville super-operator,

$$\mathcal{L}_i\left[\hat{\rho}\right]=\int d^2\boldsymbol{x}\left[2\hat{A}_i\hat{\rho}\hat{A}_i^{\dagger}-\hat{\rho}\hat{A}_i^{\dagger}\hat{A}_i-\hat{A}_i^{\dagger}\hat{A}_i\hat{\rho}\right], \tag{2.9}$$

describes the output coupling of the i-th intracavity mode with the external bath.

We note that, although we focus on the master equation approach here, it is sometimes useful to write the time evolution in a complementary quantum Langevin formulation. This formulation is given in Appendix A.

III. STOCHASTIC EQUATIONS IN THE POSITIVE-P REPRESENTATION

As nonlinear operator equations are not generally soluble, it is more manageable to map the operator equations into c-number form. In this approach, a master equation is transformed into a positive-definite Fokker-Planck equation using operator identities that map the operator terms in the master equation into differential operators [43, 45, 48]. To do this we have to use a phase-space representation of the master equation.

Phase-space representations in a classical phase-space do not give a positive-definite equation. An example is the Wigner representation [49]. While this is exact, it is not able to be mapped into Langevin equations, unless one either truncates or uses higher order noise [50]. One can also linearize the Hamiltonian and obtain an approximate Wigner diffusion [38]. Another approach is the Husimi Q-function [51], where, in order to obtain a positive Fokker-Planck equation, an unphysical constraint on the phase-space trajectories has to be used [52].

Here we wish to have the ability to treat non-equilibrium structures without restrictions. For this purpose, the most useful representation is the positive-P representation [40], which is an extension of the Glauber-Sudarshan P-representation [53] into a phase-space of double the classical dimensions. Unlike the P-representation, which is singular for nonclassical states, the positive-P representation is well-defined, positive and non-singular for any quantum state. This approach allows us to map the density matrix equation into a Fokker-Planck equation on a non-classical phase-space. In the positive-P representation stochastic averages give normally-ordered quantum expectation values. A brief description is given in Appendix B.

The stochastic field partial differential equations are given by an extension of our earlier work [23]:

$$\begin{aligned}
\frac{\partial A_0}{\partial t}&=-\tilde{\gamma}_0A_0+\mathcal{E}(\boldsymbol{x})-\chi^*A_1A_2+\frac{iv_0^2}{2\omega_0}\nabla^2A_0\,,\\
\frac{\partial A_1}{\partial t}&=-\tilde{\gamma}_1A_1+\chi A_0A_2^{+}+\frac{iv_1^2}{2\omega_1}\nabla^2A_1+\sqrt{\chi A_0}\xi_1\,,\\
\frac{\partial A_2}{\partial t}&=-\tilde{\gamma}_2A_2+\chi A_0A_1^{+}+\frac{iv_2^2}{2\omega_2}\nabla^2A_2+\sqrt{\chi A_0}\xi_2\,.
\end{aligned} \tag{3.1}$$

The three equations that correspond to the hermitian conjugate fields, A_i^+, are obtained by conjugating the constant terms, and replacing stochastic and noise fields so that: $A_i\to A_i^+$ and $\xi_i\to\xi_i^+$, where ξ_i and ξ_i^+ are independent Gaussian complex noises. These are equivalent in the mean to the conjugated Heisenberg equations, but are independent c-number equations. They are not conjugate in every realization. We also note that A_i and A_i^+ are six independent, complex c-number fields.

The stochastic fields ξ_k that describe the quantum noise are complex and Gaussian, whose non-vanishing correlations are:

$$\begin{aligned}
\left\langle\xi_1(\boldsymbol{x},t)\xi_2(\boldsymbol{x}',t')\right\rangle&=\delta^2(\boldsymbol{x}-\boldsymbol{x}')\delta(t-t')\\
\left\langle\xi_1^+(\boldsymbol{x},t)\xi_2^+(\boldsymbol{x}',t')\right\rangle&=\delta^2(\boldsymbol{x}-\boldsymbol{x}')\delta(t-t')\,.
\end{aligned} \tag{3.2}$$

This means that $\xi_k(\boldsymbol{x},t)$, $\xi_k^+(\boldsymbol{x},t)$ represent four independent, delta-correlated, complex c-number Gaussian stochastic fields with zero mean. They are completely characterized by the specified correlations. From the stochastic equations (3.1), it is clear that the amplitude of the stochastic fluctuations that act on the converted modes depend on the pump field dynamics. A brief discussion of the noises is given in Appendix B.

A. Critical driving field

As a first investigation, we treat the classical approximation, which has also been analyzed in some earlier work [24, 31, 54–57]. Here one assumes that all noise is negligible, so that $A_i^+=A_i^*$, which gives equations in the form:

$$\begin{aligned}
\frac{\partial A_0}{\partial t}&=-\tilde{\gamma}_0A_0+\mathcal{E}(\boldsymbol{x})-\chi^*A_1A_2+\frac{iv_0^2}{2\omega_0}\nabla^2A_0\,,\\
\frac{\partial A_i}{\partial t}&=-\tilde{\gamma}_iA_i+\chi A_0A_{3-i}^*+\frac{iv_i^2}{2\omega_i}\nabla^2A_i\,.
\end{aligned} \tag{3.3}$$

The phases of $\mathcal{E}$ and χ are essentially arbitrary, as they depend on the phase definition for the field amplitudes A_i, which in turn depend on arbitrary mode phases. We will use this freedom later on to simplify the equations. If in addition, we assume that the input is a plane-wave, and we ignore possible spatial instabilities, diffraction can

be neglected as well. A steady-state result involves setting the time-derivatives to zero, so:

$$A_0 = \left(\mathcal{E} - \chi^* A_1 A_2\right)/\tilde{\gamma}_0\,,$$
$$A_i = \chi A_0 A_{3-i}^*/\tilde{\gamma}_i\,. \tag{3.4}$$

Hence, the defining equation for a steady-state is:

$$A_1 A_2^* = \frac{A_1 A_2^* \left|\chi A_0\right|^2}{\tilde{\gamma}_1 \tilde{\gamma}_2^*}\,. \tag{3.5}$$

We can always choose the interaction picture detuning ϵ so that $\tilde{\gamma}_1\tilde{\gamma}_2^* = \bar{\gamma}^2$ is real, otherwise the above threshold solutions will be oscillatory rather than stable. There are two types of steady-state solution. Either $A_1 A_2^* = 0$, or else $|\chi A_0| = \bar{\gamma}$. The first is called a below-threshold solution, the second an above-threshold solution. There is a driving field where both the solutions coincide, at a critical pump intensity of:

$$\left|\mathcal{E}_c\right|^2 = \bar{\gamma}^2\left|\tilde{\gamma}_0/\chi\right|^2\,. \tag{3.6}$$

More generally, suppose we are in the above-threshold regime. Using Eq. (3.4), and defining $A_1^* A_1 = I_1$, one obtains:

$$A_0 = \left(\mathcal{E} - \left|\chi^2\right| I_1 A_0/\tilde{\gamma}_2\right)/\tilde{\gamma}_0\,. \tag{3.7}$$

On re-arranging the equation, and using the above-threshold solution $|\chi A_0| = \bar{\gamma}$, this result becomes:

$$\left|\chi A_0\right|^2 = \bar{\gamma}^2 = \frac{\left|\tilde{\gamma}_2\chi\mathcal{E}\right|^2}{\left|\tilde{\gamma}_0\tilde{\gamma}_2 + \left|\chi^2\right| I_1\right|^2}\,. \tag{3.8}$$

The roots of the resulting quadratic are:

$$I_1 = \frac{1}{\left|\chi^2\right|}\left[-z' \pm \sqrt{\left|\chi\mathcal{E}\right|^2 + \left(z'\right)^2 - \left|z\right|^2}\right]\,, \tag{3.9}$$

where $z = z' + iz'' = \tilde{\gamma}_0\tilde{\gamma}_2$.

Solutions with negative intensities are unphysical. There is a positive, above-threshold solution if $|\chi\mathcal{E}| > |z|$, which gives an identical critical field to Eq. (3.6). For $|\mathcal{E}| > \mathcal{E}_c$ there is a transfer of energy from the pump to the signal and idler modes, which develop a finite mean intensity. It is the vicinity and just above this critical point that is the main regime of interest in this paper. We note that above threshold, further instabilities exist, including limit cycles and spatial pattern formation [56].

IV. ADIABATIC ELIMINATION OF THE PUMP MODE

We now return to the full quantum behavior given by the stochastic equations obtained above. One limit that has an especially simple behavior is found in the case of a rapidly decaying pump mode. We can treat this by means of an adiabatic elimination procedure. Assuming that $\tilde{\gamma}_0 \gg \tilde{\gamma}_1 \simeq \tilde{\gamma}_2$, and that $\mathcal{E}$ is spatially uniform (that is, we are neglecting pump diffraction), we can perform an adiabatic elimination by using the stationary solution for the pump mode, so that

$$A_0 = \bar{A}_0 \equiv \frac{\mathcal{E} - \chi^* A_1 A_2}{\tilde{\gamma}_0}\,. \tag{4.1}$$

A. Signal and idler equations

The resulting equations for the down-converted modes - often called the signal and idler equations - are, for $i = 1, 2$:

$$\frac{\partial A_i}{\partial t}(\boldsymbol{x}, t) = -\tilde{\gamma}_i A_i + \frac{\chi}{\tilde{\gamma}_0}\left(\mathcal{E} - \chi^* A_1 A_2\right) A_{3-i}^+ + \\ + \frac{iv_i^2}{2\omega_i}\nabla^2 A_i + \sqrt{\chi\bar{A}_0}\xi_i(\boldsymbol{x}, t)\,. \tag{4.2}$$

We see that the main effect of detuning the pump is to reduce the effective intra-cavity pump intensity. So far, we have treated the case of general frequencies and group velocities. An important special case is obtained when the two down-converted frequencies are equal. In this case, the modes are still non-degenerate, as they can have different polarizations. From now on, we consider this special case for simplicity, so we take $\tilde{\gamma}_1 = \tilde{\gamma}_2 = \tilde{\gamma}$, $v_1 = v_2 = v$ and $\omega_1 = \omega_2 = \omega$. This implies that $\Delta_1 = \Delta_2 = \Delta$. We will also assume that $\Delta_0 = 0$, i.e. that the pump is on-resonance with the cavity, even when the down-converted fields may be off-resonant from their cavity resonance frequencies.

Although these assumptions simplify the algebra, they are not essential for our main conclusions, which mostly rely simply on the fact that we now have a two-dimensional order parameter rather than a one-dimensional order parameter as found in the degenerate case. We should note that a non-zero pump detuning can excite another modes different from ω_0. This could give rise to nonlinear phenomena like bistabilities, nonlinear resonances and subcritical bifurcation, especially for the case of large detuning [24]. In the case where the diffraction terms are different, there will be a new term which is proportional to the difference of the two diffraction terms, as has been studied elsewhere [24]. This term will be present in the equations even for the case of zero detuning. Since we are interesting in the universal behaviour of the system we do not include these cases, but we point out that they can give rise to nonlinear behaviour.

B. Dimensionless form

Equation (4.2) will now be transformed into a dimensionless form which allows comparisons with other types of phase transitions. First, we define the dimensionless variables $\tau = t/t_0$, $\boldsymbol{r} = \boldsymbol{x}/x_0$, with a scaled Laplacian

$\nabla^2_{\boldsymbol{r}} = \partial^2/\partial r_1^2 + \partial^2/\partial r_2^2$. It is useful to also define a dimensionless field $\alpha_i = x_0 A_i$ as well. This has an intuitive interpretation as the coherent amplitude in real space, defined relative to a physical area of x_0^2. After this transformation, one obtains:

$$\frac{1}{t_0}\frac{\partial \alpha_i}{\partial \tau} = -\tilde{\gamma}\alpha_i + \chi \bar{A}_0 \alpha^+_{3-i} + \frac{iv^2}{2\omega x_0^2}\nabla^2_{\mathbf{r}}\alpha_i + x_0\sqrt{\chi \bar{A}_0}\xi_i\,. \tag{4.3}$$

We define $\tilde{\gamma} = \gamma\,(1 + i\Delta)$ and introduce the dimensionless pump amplitude

$$\tilde{\mu} = \frac{\chi \mathcal{E}}{\gamma_0 \gamma} = \mu e^{i\phi}\,, \tag{4.4}$$

where μ is real and positive. Since the phase of the driving field $\mathcal{E}$ is arbitrary, and the equations are invariant under phase-changes of $\mathcal{E}$, we will choose $\phi = 0$ with no loss of generality. We also define the time-scale $t_0 = 1/g\gamma$ as the scaling time for critical slowing down, where

$$g^2 = \frac{|\chi|^2}{4\gamma_0 \gamma x_0^2}\,. \tag{4.5}$$

The length scale x_0 is now chosen so that:

$$x_0^2 = \frac{v^2}{2\gamma\sqrt{g}\omega}\,. \tag{4.6}$$

Combining Eqs. (4.5) and (4.6), one can write the dimensionless coupling g in the form:

$$g = \left(\frac{|\chi|^2\,\omega}{2\gamma_0 v^2}\right)^{2/3}\,. \tag{4.7}$$

Similarly, we introduce dimensionless complex noises $\zeta_i = \xi_i x_0\sqrt{t_0}$, so that

$$\begin{aligned}\langle \zeta_1(\boldsymbol{r},\tau)\zeta_2(\boldsymbol{r}\,',\tau')\rangle &= \delta^2(\boldsymbol{r}-\boldsymbol{r}\,')\delta(\tau-\tau'),\\ \left\langle \zeta_1^+(\boldsymbol{r},\tau)\zeta_2^+(\boldsymbol{r}\,',\tau')\right\rangle &= \delta^2(\boldsymbol{r}-\boldsymbol{r}\,')\delta(\tau-\tau').\end{aligned} \tag{4.8}$$

Finally, defining the driving field saturation factor as:

$$\begin{aligned}\mu\,(\vec{\alpha}) &= \mu - 4g^2\alpha_1\alpha_2,\\ \mu^+\,(\vec{\alpha}) &= \mu - 4g^2\alpha_1^+\alpha_2^+,\end{aligned} \tag{4.9}$$

we obtain the following dimensionless form of the scaled equations for $i = 1, 2$:

$$\begin{aligned}g\frac{\partial \alpha_i}{\partial \tau} &= \mu\,(\vec{\alpha})\,\alpha^+_{3-i} - (1 + i\Delta)\,\alpha_i\\ &\quad + \sqrt{g}\left[i\nabla^2_{\boldsymbol{r}}\alpha_i + \sqrt{\mu\,(\vec{\alpha})}\zeta_i(\boldsymbol{r},\tau)\right],\end{aligned} \tag{4.10}$$

together with a conjugate equation for α_i^+. Although this is true in general, we are mostly interested here in the regime of $g \ll 1$, which allows us to make an expansion in powers of the coupling. For small g, the classical approximation gives the leading order term, while the diffraction and noise terms provide the next order in an expansion in $\sqrt{g}$.

V. STABILITY PROPERTIES AND QUADRATURE EQUATIONS

We now wish to transform these equations into quadrature equations that are simpler to investigate. There are very different stability properties for the orthogonal quadratures near the critical point. To investigate this, as a first approximation, we will ignore noise and nonlinear terms of order $\sqrt{g}$ and smaller. The stability of the equations near $\alpha_i = 0$, to leading order in g, is:

$$g\frac{\partial}{\partial \tau}\begin{pmatrix}\alpha_1\\ \alpha_2^+\end{pmatrix} = \begin{pmatrix}-(1+i\Delta) & \mu\\ \mu & -(1-i\Delta)\end{pmatrix}\begin{pmatrix}\alpha_1\\ \alpha_2^+\end{pmatrix}, \tag{5.1}$$

which has eigenvalues $\lambda_\pm = -1 \pm \sqrt{-\Delta^2 + \mu^2}$, and with a similar equation coupling α_2 and α_1^+. This gives an unstable eigenvalue, leading classically to growth of the signal and idler terms if $\mu^2 - \Delta^2 > 1$, as expected from the analysis in the previous section. The resulting eigenvectors, $\vec{u}_\pm$, are:

$$\vec{u}_\pm = \begin{pmatrix}\mu\\ i\Delta \pm \sqrt{-\Delta^2 + \mu^2}\end{pmatrix}. \tag{5.2}$$

There is clearly a line of critical points where the stability has a continuous change at $\mu^2 - \Delta^2 = 1$. The tricritical point then occurs when $\mu = 1, \Delta = 0$, as we will show in later sections.

A. Quadrature field variables

To understand the behavior of Eq. (4.10) in the neighborhood of the critical point, we define complex, dimensionless scaled quadrature fields which are proportional to the critical eigenvectors, as follows [23, 38]:

$$\begin{aligned}X &= \sqrt{g}\left(\alpha_1 + \alpha_2^+\right),\\ X^+ &= \sqrt{g}\left(\alpha_2 + \alpha_1^+\right),\\ Y &= \frac{1}{i}\left(\alpha_1 - \alpha_2^+\right),\\ Y^+ &= \frac{1}{i}\left(\alpha_2 - \alpha_1^+\right).\end{aligned} \tag{5.3}$$

Next, we consider the case $\mu \approx 1 \gg g^2\,|\alpha_1\alpha_2|$, to simplify the noise term. As this is both relatively small, and nearly constant in the neighborhood of the critical point, the resulting terms are of higher order in g than the leading terms we wish to include. The resulting equations for these quadratures in the positive P-representation near

the critical point are:

$$\begin{aligned}
\frac{\partial X}{\partial \tau} &= \frac{\mu_-}{g}X + \mathcal{D}_+ Y - \left(X^2 + gY^2\right)X^+ + \zeta_+.\\
\frac{\partial X^+}{\partial \tau} &= \frac{\mu_-}{g}X^+ + \mathcal{D}_+ Y^+ - \left(X^{+2} + gY^{+2}\right)X + \zeta_+^*.\\
g\frac{\partial Y}{\partial \tau} &= -\mu_+ Y + \mathcal{D}_- X - g\left(X^2 + gY^2\right)Y^+ - i\sqrt{g}\zeta_-.\\
g\frac{\partial Y^+}{\partial \tau} &= -\mu_+ Y^+ + \mathcal{D}_- X^+ - g\left(X^{+2} + gY^{+2}\right)Y - i\sqrt{g}\zeta_-^*.
\end{aligned} \tag{5.4}$$

Here we have defined a modified Laplacian and driving term as:

$$\begin{aligned}
\mathcal{D}_\pm &= \pm\frac{\Delta}{\sqrt{g}} \mp \nabla_{\boldsymbol{r}}^2\\
\mu_\pm &= \mu \pm 1.
\end{aligned} \tag{5.5}$$

and new Gaussian noise terms according to:

$$\zeta_\pm = \zeta_1 \pm \zeta_2^+ = \left(\zeta_2 \pm \zeta_1^+\right)^*, \tag{5.6}$$

where we have used the result of Eq. (C5). This shows that the noise terms driving the X, X^+ fields are conjugate, while those driving the Y, Y^+ fields change sign on conjugation, so that Y, Y^+ will not remain conjugate during time-evolution.

At this stage, we can make the following remarks. The stochastic quadrature fields X, X^+ are both complex fields, so they have four degrees of freedom between them, and similarly for Y, Y^+. They have a correspondence with non-Hermitian operator fields $\hat{X}$, $\hat{X}^\dagger$ and $\hat{Y}$, $\hat{Y}^\dagger$. In general, Y, Y^+ are not complex conjugate except in the mean, and neither are X, X^+, since they are driven by the Y, Y^+ fields. However, as we will show, this picture simplifies when one considers an expansion near the critical point.

B. Critical point adiabatic elimination

We can now perform a second type of adiabatic elimination which is valid in the neighborhood of the critical point. This takes into account the fact that the fluctuations in the X quadrature become very slow near threshold, while the Y quadrature still responds on the fast relative time scale $1/\gamma$. Formally, we can drop terms of $\mathcal{O}(\sqrt{g})$ where $g \ll 1$, and approximate equations (5.4) as follows [23]:

$$\begin{aligned}
\frac{\partial X}{\partial \tau} &= -\left(\frac{1-\mu}{g}\right)X + \left(\frac{\Delta}{\sqrt{g}} - \nabla_{\boldsymbol{r}}^2\right)Y - X^2X^+ + \zeta_+\,,\\
\frac{\partial X^+}{\partial \tau} &= -\left(\frac{1-\mu}{g}\right)X^+ + \left(\frac{\Delta}{\sqrt{g}} - \nabla_{\boldsymbol{r}}^2\right)Y^+ - X^{+2}X + \zeta_+^*\,,\\
0 &= -(1+\mu)Y + \nabla_{\boldsymbol{r}}^2 X\,,\\
0 &= -(1+\mu)Y^+ + \nabla_{\boldsymbol{r}}^2 X^+.
\end{aligned} \tag{5.7}$$

Here we have considered that the noise term of the quadrature variables Y, Y^+ has been neglected since it scales as $\sqrt{g}$ and we are considering the limit $g \ll 1$. If this limit is not taken, the noise term would appear in the above equations. To lowest order in g, we can eliminate the fast or non-critical quadrature Y, Y^+ variables by setting:

$$Y^{(+)} = \frac{\nabla^2 X^{(+)}}{1+\mu}\,, \tag{5.8}$$

which gives the result that:

$$\begin{aligned}
\frac{\partial X}{\partial \tau} &= \tilde{\mathcal{D}}X - X^2X^+ + \zeta_+\,,\\
\frac{\partial X^+}{\partial \tau} &= \tilde{\mathcal{D}}X - \left(X^+\right)^2 X + \zeta_+^*.
\end{aligned} \tag{5.9}$$

Here we have introduced a linear differential operator that describes the linear gain, loss and diffraction terms:

$$\tilde{\mathcal{D}} \equiv \tilde{\mathcal{D}}_r = -\eta_1 + \eta_2\nabla_{\boldsymbol{r}}^2 - \eta_3\nabla_{\boldsymbol{r}}^4 \tag{5.10}$$

where we have defined the following parameters:

$$\begin{aligned}
\eta_1 &= \left(\frac{1-\mu}{g}\right),\\
\eta_2 &= \frac{\Delta}{(1+\mu)\sqrt{g}},\\
\eta_3 &= \frac{1}{1+\mu}.
\end{aligned} \tag{5.11}$$

We note that since the non-conjugate variables Y, Y^+ do not appear in these equations, it follows that variables X, X^+ will remain conjugate if they are conjugate initially, as for example in an initial thermal or coherent state. Hence, to leading order, we can set $X^+ = X^*$ near the critical point, and write one complex equation for the critical quadratures, which is valid near threshold:

$$\frac{\partial X}{\partial \tau} = \tilde{\mathcal{D}}X - X\left|X\right|^2 + \zeta_+\,. \tag{5.12}$$

While this equation is similar to a Landau-Ginzburg equation for a complex order parameter [58], it is not identical, owing to the presence of the fourth-order Laplacian term in $\tilde{\mathcal{D}}$. In the next section we will show that the equations are similar to a vector Swift-Hohenberg equation [2].

C. Vector Swift-Hohenberg equations

We will now show that these near-threshold equations are actually coupled or vector Swift-Hohenberg equations [2] that represent the leading order dynamics near threshold of the down-converted modes with the same frequency but orthogonal polarization. To demonstrate this, it is convenient to make the following change of variables:

$$X_1 = \frac{X + X^*}{2}, \qquad X_2 = \frac{X - X^*}{2i}. \tag{5.13}$$

After this change of variables it is possible to write the equation (5.12) as a single vector equation, as we now show. On inverting this equation we get:

$$X = X_1 + iX_2, \qquad X^* = X_1 - iX_2. \tag{5.14}$$

Next we define define two real vectors $\boldsymbol{X}$ and $\tilde{\boldsymbol{\zeta}}$ as:

$$\boldsymbol{X} = \begin{pmatrix} X_1 \\ X_2 \end{pmatrix}, \qquad \tilde{\boldsymbol{\zeta}} = \frac{1}{2}\begin{pmatrix} \zeta_+ + \zeta_+^* \\ i\left(\zeta_+ - \zeta_+^*\right) \end{pmatrix}.$$

Using the above expressions we can write Eq. (5.12) as a single vector equation of the form:

$$\frac{\partial \boldsymbol{X}}{\partial \tau} = \tilde{\mathcal{D}}\boldsymbol{X} - |\boldsymbol{X}|^2 \boldsymbol{X} + \tilde{\boldsymbol{\zeta}}, \tag{5.15}$$

where $\boldsymbol{X}$ is a two real component vector whose elements are X_1 and X_2, and $\tilde{\boldsymbol{\zeta}}$ is also a two real component Gaussian noise vector, with correlations given by:

$$\left\langle \tilde{\zeta}_i(\boldsymbol{r},\tau)\tilde{\zeta}_j(\boldsymbol{r}',\tau')\right\rangle = \delta_{ij}\delta(\boldsymbol{r}-\boldsymbol{r}')\delta(\tau-\tau'). \tag{5.16}$$

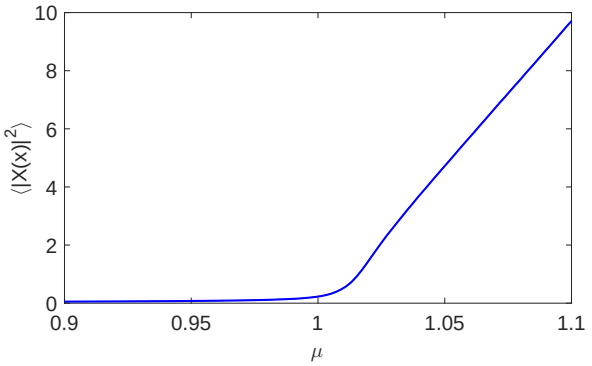

Figure 1. Dimensionless intensity versus dimensionless pump μ in the vicinity of the critical point. The point $\mu = 1$ corresponds to $\eta_1 = \eta_2 = 0$ and $\eta_3 = \frac{1}{2}$. Here we have used the parameter $g = 0.01$. Results were obtained from a simulation with 300 samples on a $50 \times 20 \times 20$ numerical grid of $30000 \times 96 \times 96$ points.

In Fig. (1) we plot the modulus squared of the two-dimensional order parameter $\boldsymbol{X}$ vs the dimensionless pump parameter μ, averaged over a transverse area of dimensionless size 20×20.

Direct simulations were employed, using both a central partial difference algorithm in the interaction picture [59] and a fourth order interaction picture Runge-Kutta method. Two public domain software packages were used and checked against each other [60]. This figure is obtained by solving the stochastic equations given in Eq. (5.15) at $\mu = 0.9$, equilibrating for $t = 50$ units then scanning the driving field μ adiabatically (using $\mu = 0.9 + 0.004t$) through the critical point until $\mu = 1.1$. There is a rate-independent critical region at the threshold value of $\mu = 1$, where the transition is smooth rather than discontinuous, as it would be classically.

In the case of a one-dimensional, real order parameter, this equation was first derived by Swift and Hohenberg [2, 3, 61]. Here it appears as a two-dimensional vector equation, since the order parameter is two-dimensional. This was used to explain the convective roll patterns generated by the Rayleigh-Bénard instability, where the order parameter is the vertical fluid velocity. The real order parameter case is also similar to the Ising model for magnets in two dimensions with next nearest neighbor interactions [62], where competition between the nearest and next nearest interactions generates a magnetic modulated phase called the Lifshitz phase [22].

Higher dimensional or complex order parameters, as in the present analysis, are described using a generalized Landau-Ginzburg-Wilson Hamiltonian [28], where the authors also introduce the Lifshitz point. For the present case, the upper critical dimension for classical behavior is at $d = 5$, and the classical location of the Lifshitz point is at $\eta_1 = \eta_2 = 0$. Low dimensional cases should have enhanced fluctuations, without spontaneous magnetization or symmetry breaking, as expected from the Mermin-Wagner theorem [39]. This applies to Heisenberg-type models with higher-dimensional order parameters in two dimensions. As it is valid for general, finite-range interactions, it also holds in our case.

VI. CORRELATIONS

All physical quantities that we wish to understand in the double adiabatic limit treated in the previous section, come from the solution of equation (5.15). This allows us to calculate the expectation value of any other observable in the vicinity of the critical point. Another way to obtain expectation values is write the functional probability as a solution of the master equation. Below we develop both methods.

A. Stationary solution of the Fokker Planck equation

We start with equation (5.15) and note that it is possible to write a functional Fokker-Planck equation for the probability density $P(\boldsymbol{X},\tau)$,

$$\frac{\partial P}{\partial \tau}(\boldsymbol{X},\tau) = \sum_i \frac{\delta}{\delta X_i}\left[\left(|\boldsymbol{X}|^2 - \tilde{\mathcal{D}}\right)X_i + \frac{1}{2}\frac{\delta}{\delta X_i}\right]P(\boldsymbol{X},\tau) \tag{6.1}$$

and look for the equilibrium distribution in the form $P(\boldsymbol{X}) = N\exp[-\mathcal{H}(\boldsymbol{X})]$, where $\mathcal{H}$ is a potential function. The solution for the distribution of $\boldsymbol{X}$ is given by:

$$P(\boldsymbol{X}) = N\exp\left[-\int d^2x\left(\eta_1\boldsymbol{X}\cdot\boldsymbol{X} + \frac{1}{2}(\boldsymbol{X}\cdot\boldsymbol{X})^2 + \right.\right.$$
$$\left.\left. + \eta_2\nabla\boldsymbol{X}\cdot\nabla\boldsymbol{X} + \eta_3\nabla^2\boldsymbol{X}\cdot\nabla^2\boldsymbol{X}\right)\right]. \tag{6.2}$$

This expression is similar to the Landau-Ginzburg free energy of a next nearest neighbor interaction in a planar

magnetic interaction, with $\boldsymbol{X}$ playing the role of a two component vector order parameter. Owing to this parallel, the planar type-II parametric system can provide a superb model platform for investigating fluctuations and universal behavior in this paradigmatic system.

B. Stochastic moments in the Gaussian approximation

In order to evaluate the moments and spatial correlations we will approximate the nonlinear terms of Eq. (5.15) using a Gaussian approximation together with a Green's function approach. Hence we can write Eq. (5.15) as follows:

$$\frac{\partial \left\langle X_i(\boldsymbol{r},\tau)X_j(\boldsymbol{r}',\tau)\right\rangle}{\partial\tau} = \tilde{\mathcal{D}}_r \left\langle X_i(\boldsymbol{r},\tau)X_j(\boldsymbol{r}',\tau)\right\rangle - \left\langle X_i(\boldsymbol{r},\tau)\left|\boldsymbol{X}\left(\boldsymbol{r},\tau\right)\right|^2 X_j(\boldsymbol{r}',\tau)\right\rangle. \tag{6.3}$$

Here $\langle\ldots\rangle$ denotes the stochastic average over the Gaussian fluctuations and we have used the notation $\tilde{\mathcal{D}}_r$ in order to avoid ambiguities. We explicitly denote that the operator $\tilde{\mathcal{D}}$ acts on the spatial coordinate r. In the Gaussian approximation, fluctuations around the most probable configuration are approximately treated as independent modes with Gaussian distributions [63]. This allows us to replace ensemble averages by a Gaussian ansatz, in which higher order moments are approximated by the expressions for a Gaussian distribution, e.g. $\langle X^4\rangle \simeq 3\langle X^2\rangle^2$. On defining $G_{ij} \equiv G_{ij}\left(\boldsymbol{r},\boldsymbol{r}'\right) = \langle X_i(\boldsymbol{r},\tau)X_j(\boldsymbol{r}',\tau)\rangle$ we can write the above equation, for $i=1$, as:

$$\frac{\partial G_{1j}}{\partial\tau} = \tilde{\mathcal{D}}_r G_{1j} - G_{1j}\left(3\left\langle X_1^2\right\rangle + \left\langle X_2^2\right\rangle\right).$$

Here we have assumed rotational symmetry of the problem in the (X_1, X_2) plane, so that $\langle X_1X_2\rangle = 0$. Using again the assumption of rotational symmetry in the $X_1 - X_2$ plane, we can also write the Green's function results as:

$$\frac{\partial G_{1j}}{\partial\tau} = \left[\tilde{\mathcal{D}}_r - 2\left(\left\langle X_1^2\right\rangle + \left\langle X_2^2\right\rangle\right)\right] G_{1j}. \tag{6.4}$$

This corresponds to an equivalent stochastic equation, valid in the steady-state for a rotationally symmetric system:

$$\frac{\partial\tilde{\boldsymbol{X}}(\boldsymbol{r},\tau)}{\partial\tau} = \tilde{\mathcal{D}}\tilde{\boldsymbol{X}}(\boldsymbol{r},\tau) - 2\left\langle\tilde{\boldsymbol{X}}\cdot\tilde{\boldsymbol{X}}\right\rangle\tilde{\boldsymbol{X}}(\boldsymbol{r},\tau) + \tilde{\boldsymbol{\zeta}}(\boldsymbol{r},\tau). \tag{6.5}$$

We use the variable $\tilde{\boldsymbol{X}}$ to denote that we are using the Gaussian approximation. In order to evaluate the Gaussian correlation functions in near and far field, we will define a parameter $\eta_1' = \eta_1 + 2\langle\tilde{\boldsymbol{X}}\cdot\tilde{\boldsymbol{X}}\rangle$. Using the expression for $\tilde{\mathcal{D}}$ of Eq. (5.10) we can write the above equation as:

$$\frac{\partial\tilde{\boldsymbol{X}}(\boldsymbol{r},\tau)}{\partial\tau} = \left(-\eta_1' + \eta_2\nabla_{\boldsymbol{r}}^2 - \eta_3\nabla_{\boldsymbol{r}}^4\right)\tilde{\boldsymbol{X}}(\boldsymbol{r},\tau) + \tilde{\boldsymbol{\zeta}}(\boldsymbol{r},\tau). \tag{6.6}$$

Next, we note that because of translational symmetry the term $\left\langle\tilde{\boldsymbol{X}}\cdot\tilde{\boldsymbol{X}}\right\rangle$ is independent of the spatial coordinate so that $\left\langle\tilde{\boldsymbol{X}}\cdot\tilde{\boldsymbol{X}}\right\rangle = \left\langle\left|\tilde{X}\right|^2\right\rangle$ can be calculated analytically. In order to evaluate it, we use the Fourier transform

$$\tilde{\boldsymbol{X}}(\boldsymbol{r},t) = \frac{1}{2\pi}\int e^{i\vec{k}\cdot\boldsymbol{r}}\tilde{\boldsymbol{X}}(\vec{k},t)d^2\vec{k}, \tag{6.7}$$

so that in momentum space we write Eq. (6.6) as:

$$\frac{\partial\tilde{\boldsymbol{X}}(\boldsymbol{k},\tau)}{\partial\tau} = -\left(\eta_1' + \eta_2k^2 + \eta_3k^4\right)\tilde{\boldsymbol{X}}(\boldsymbol{k},\tau) + \tilde{\boldsymbol{\zeta}}(\boldsymbol{k},\tau). \tag{6.8}$$

C. Lifshitz point

We now consider the line of points where $\eta_2 = 0$ and $\eta_3 = \frac{1}{2}$. These are the points we have defined as corresponding physically to zero detuning, with a pump in the vicinity of the $\mu = 1$. In this case the solution for $\tilde{\boldsymbol{X}}(\vec{k},t)$ is given by:

$$\tilde{\boldsymbol{X}}(\boldsymbol{k},\tau) = \int_{-\infty}^{\tau}\tilde{\boldsymbol{\zeta}}(\boldsymbol{k},\tau')e^{-\left(\eta_1'+\frac{k^4}{2}\right)(\tau-\tau')}d\tau'. \tag{6.9}$$

In this way, we obtain:

$$\left\langle\tilde{\boldsymbol{X}}\cdot\tilde{\boldsymbol{X}}\right\rangle = \frac{1}{4\pi^2}\int_0^\infty\frac{2\pi kdk}{\eta_1'+\frac{k^4}{2}}. \tag{6.10}$$

On performing the integration there is a resulting self-consistency condition:

$$\left\langle\tilde{\boldsymbol{X}}\cdot\tilde{\boldsymbol{X}}\right\rangle = \frac{1}{4\sqrt{2(\eta_1 + 2\left\langle\tilde{\boldsymbol{X}}\cdot\tilde{\boldsymbol{X}}\right\rangle)}}. \tag{6.11}$$

At the Lifshitz point, where $\eta_1 = 0$, we find that:

$$\left\langle\tilde{\boldsymbol{X}}\cdot\tilde{\boldsymbol{X}}\right\rangle = \langle\left|\tilde{X}\right|^2\rangle = 0.25. \tag{6.12}$$

As explained below, this is remarkably close to accurate numerical simulations of the correlations, including non-Gaussian fluctuations.

We also consider the case where $\mu = 1$, $\eta_2 \neq 0$ and $\eta_3 = \frac{1}{2}$. This corresponds to the case of non-zero detuning Δ. In Fig. (2) we plot the modulus squared of the two dimensional order parameter $\boldsymbol{X}$ vs the detuning Δ.

In order to obtain this figure, we solve the stochastic equations given in Eq. (5.15), and scan the detuning which is proportional to the parameter η_2 defined in Eq. (5.11), so that $\Delta = -0.5 + 0.005t$. We notice that the

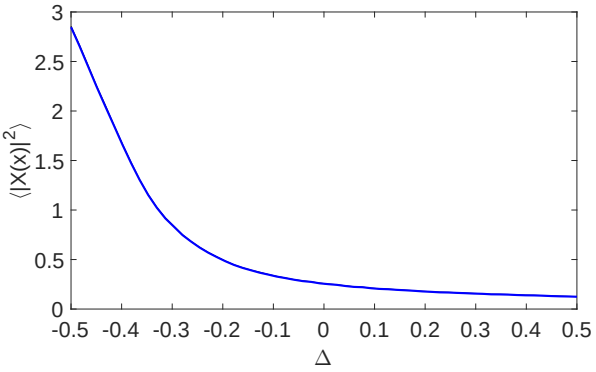

Figure 2. Dimensionless intensity versus detuning Δ. The Lifshitz point corresponds to zero detuning. Here we have used $\mu = 1$ and $g = 0.01$. Results were obtained from a simulation with 60 samples on a $200 \times 50 \times 50$ numerical grid of $15000 \times 96 \times 96$ points.

fluctuations depends on the detuning. For a positive detuning there is a decrease of the fluctuations while for a negative detuning the fluctuations increase. A classical Swift–Hohenberg equation with a complex order parameter and nonzero detuning has been treated [64], as has the hyperbolic complex Swift–Hohenberg equation[65] and other related studies [66, 67]. For negative detuning there is a ring with strong fluctuations, shown in figures (3) and (4).

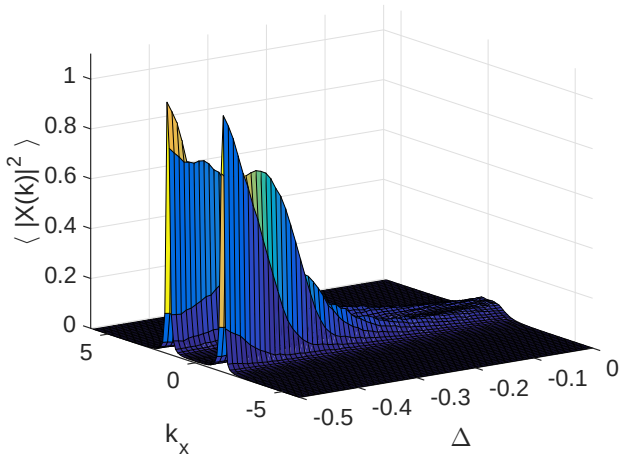

Figure 3. Dimensionless intensity versus detuning Δ and transverse momentum k_x. For negative detuning there is are fluctuations for lower momentum values. Results were obtained from a simulation with 800 samples on a $100 \times 50 \times 50$ numerical grid of $15000 \times 96 \times 96$ points. Here we have used $\mu = 1$ and $g = 0.01$.

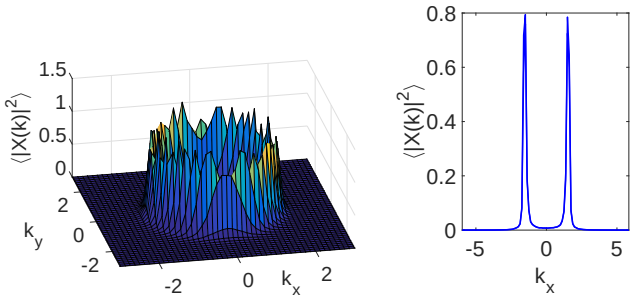

Figure 4. Left: Dimensionless intensity versus transverse momentum $\mathbf{k}$ for a fixed value of the detuning $\Delta = 0.5$. Here we have used $\mu = 1$ and $g = 0.01$. A ring is formed for lower values of the momentum. The fluctuations (peaks) are not symmetric due to noise. Right: Dimensionless intensity versus transverse momentum k_x for a fixed value of the detuning $\Delta = 0.45$, and $k_y = 0$. Other parameters are as in Fig. (3).

D. Spatial correlations in the Gaussian approximation

From Eq (6.9), the Gaussian correlation function in the momentum space (far field), in the stationary regime is therefore given by:

$$\langle \tilde{\boldsymbol{X}}(\mathbf{k}) \left[\tilde{\boldsymbol{X}}(\mathbf{k}') \right]^* \rangle = \frac{1}{2} \frac{\delta(\mathbf{k} + \mathbf{k}')}{\eta_1' + \eta_2 k^2 + \eta_3 k^4}. \tag{6.13}$$

This should be readily observable experimentally, since the far-field region of the output field from the planar cavity is simply the Fourier transform of the internal cavity field. The correlation function for the enhanced quadrature in configuration space, or near field, is:

$$\langle \tilde{\boldsymbol{X}}(\boldsymbol{r}) \tilde{\boldsymbol{X}}(\boldsymbol{r}') \rangle = \frac{1}{8\pi^2} \int d^2\mathbf{k} \frac{e^{-i\mathbf{k}\cdot(\boldsymbol{r}-\mathbf{r}')}}{\eta_1' + \eta_2 k^2 + \eta_3 k^4}. \tag{6.14}$$

On integrating over the angle variable we obtain:

$$\langle \tilde{\boldsymbol{X}}(\boldsymbol{r}) \tilde{\boldsymbol{X}}(\boldsymbol{r}') \rangle = \frac{1}{4\pi} \int_0^\infty dk \frac{k J_0\left(k|\boldsymbol{r} - \boldsymbol{r}'|\right)}{\eta_1' + \eta_2 k^2 + \eta_3 k^4}, \tag{6.15}$$

where J_0 is the Bessel function of zero order. The result of the above integration is, in the limit $\eta_2 = 0$:

$$\langle \tilde{\boldsymbol{X}}(\boldsymbol{r}) \tilde{\boldsymbol{X}}(\boldsymbol{r}') \rangle = -\sqrt{\frac{\eta_3}{\eta_1'}} \frac{1}{4\pi\eta_3} \, kei\left(\left(\frac{\eta_1'}{\eta_3} \right)^{1/4} |\boldsymbol{r} - \boldsymbol{r}'| \right), \tag{6.16}$$

where $kei(x)$ is Thomson's function [68]. An interesting remark is that as $\eta_1' \to 0$, the spatial correlation decays with a power law:

$$\langle \tilde{\boldsymbol{X}}(\boldsymbol{r}) \tilde{\boldsymbol{X}}(\boldsymbol{r}') \rangle \propto |\boldsymbol{r} - \boldsymbol{r}'|^{-0.5}. \tag{6.17}$$

We note, however, that this system is predicted to have an upper critical dimension [28] with mean-field critical exponents at spatial dimension $d > 5$. Since the system is well below this critical dimension, one may expect non-Gaussian behavior that is not predicted by the approximations used in this section.

E. Non-Gaussian behavior and universality

In order to verify these analytic results and investigate non-Gaussian correlations, numerical simulations were carried out of the original stochastic partial differential equations of Eq. (5.15). Small time steps are needed to treat the quartic growth of the squared Laplacian term in momentum, together with large sample numbers to obtain a low sampling error. In initial investigations, we used a $10 \times 10 \times 10$ numerical grid of $8000 \times 64 \times 64$ points in t, x, y respectively. Employing a fine numerical grid of $16000 \times 64 \times 64$ points to check convergence in time-step, the final steady-state correlation result converged to $\langle \boldsymbol{X} \cdot \boldsymbol{X} \rangle = 0.264 \pm 0.005$. This was close to the Gaussian value, but with a relatively large sampling error.

In order to understand the quantitative difference between the exact and Gaussian results, a more precise differencing technique was used. This variance reduction or differencing technique simulates the difference between the full sample path and the Gaussian approximation [38]. The results were in agreement with a direct simulation, but gave much more rapid convergence. This was carried out as follows. First a mean field variable, $\tilde{X}$ was simulated, in the Gaussian approximation, using:

$$\frac{\partial \tilde{X}}{\partial \tau} = \tilde{\mathcal{D}}\tilde{X} - 2\tilde{X}\left\langle \left|\tilde{X}\right|^2 \right\rangle - 2\tilde{X}^* \left\langle \tilde{X}^2 \right\rangle + \zeta_+ , \quad (6.18)$$

where the averages were carried out both over a spatial numerical grid and a set of parallel trajectories. From the analytic calculations above, this should converge precisely to the analytic result of $\left\langle |\tilde{X}|^2 \right\rangle = 0.25$, which was confirmed to a numerical accuracy of $\pm 5 \times 10^{-3}$. Here we have considered that $\eta_1 = \eta_2 = 0$ and $\eta_3 = \frac{1}{2}$, corresponding to the classical Lifshitz point.

Next, the full variable X was simulated. This was achieved by introducing a difference variable defined as $\Delta_X = X - \tilde{X}$, which has the stochastic equation:

$$\frac{\partial \Delta_X}{\partial \tau} = \tilde{\mathcal{D}}X - X\left|X\right|^2 + \zeta_+ - \frac{\partial \tilde{X}}{\partial \tau} . \quad (6.19)$$

By using an identical noise source to those in the equations for the mean-field $\tilde{X}$, the difference simulation permits a more precise calculation with reduced variance. The result, shown in Figs. (5) and (6) was that, at the critical point, $\langle \boldsymbol{X} \cdot \boldsymbol{X} \rangle = 0.2574 \pm 0.0003$. This result, of much greater accuracy, only required 3200 samples with a $10 \times 20 \times 20$ numerical grid of $10000 \times 48 \times 48$ points. The discretization error was estimated from using several grids with different transverse sizes and time-steps.

In summary, the full statistical calculation gives increased critical fluctuations due to non-Gaussian effects, but this increase is relatively small. At large transverse momentum there is no measurable difference between the Gaussian and exact results, shown in Fig. (6). The deviation from the Gaussian approximation vanishes rapidly as higher order transverse momenta are investigated. Small values of this difference are observed only at zero transverse direction.

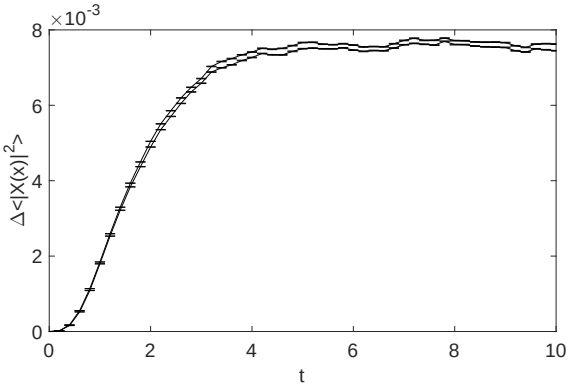

Figure 5. Growth of non-Gaussian correlations, $\langle |X|^2 - |\tilde{X}|^2 \rangle$ versus time τ, starting from $\boldsymbol{X} = 0$. Error bars were obtained from comparing a coarse (5000 step) and fine (10000 step) simulation. The sampling error is indicated by the upper and lower solid lines, with a standard deviation of ± 0.00025. This gives the steady-state correlation result $\langle \boldsymbol{X} \cdot \boldsymbol{X} \rangle = \langle |X|^2 \rangle = 0.2574 \pm 0.0003$. Results were obtained from a simulation with 3200 samples on a $10 \times 20 \times 20$ fine numerical grid of $10000 \times 48 \times 48$ points.

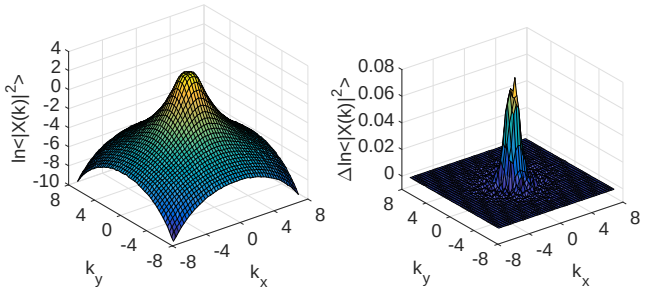

Figure 6. Left: Steady-state momentum correlations, $\langle |X(\mathbf{k})|^2 \rangle$ versus transverse momentum $\mathbf{k}$, starting from $X = 0$. Right: Steady-state non-Gaussian correlations in momentum space, $\Delta \ln \left\langle |X(\mathbf{k})|^2 \right\rangle = \ln \left\langle |X(\mathbf{k})|^2 \right\rangle - \ln \left\langle |\tilde{X}(\mathbf{k})|^2 \right\rangle$ versus momentum $\mathbf{k}$. Here we consider $\eta_1 = \eta_2 = 0$ and $\eta_3 = \frac{1}{2}$. Other parameters are as in Fig. (5)

VII. CONCLUSION

We have shown that parametric down-conversion in a type-II parametric planar cavity leads to a Swift and Hohenberg type of stochastic equation for the leading terms in the critical fluctuations, but with a vector order parameter. This combines the rotationally invariant symmetry properties of the X-Y model with the higher-order Laplacian of a Lifshitz magnetic phase transition. Surprisingly, these fluctuations are not thermal in origin, but come instead from the quantum fluctuations associated with parametric amplification.

This model can be approximately treated for the critical fluctuations with a Gaussian factorization. However, a careful numerical treatment shows that non-Gaussian critical fluctuations occur. These are responsible for enhanced intensity correlations, but are reduced at large transverse momenta due to the momentum dependence of the linear propagator. As techniques improve, we expect that this novel, non-equilibrium critical point will become accessible to experimental studies.

APPENDIX A: QUANTUM LANGEVIN FORM

In the quantum Langevin form the corresponding operator equations of the system would be:

$$\begin{aligned}
\frac{\partial \hat{A}_0}{\partial t} &= -\tilde{\gamma}_0 \hat{A}_0 + \mathcal{E}(\boldsymbol{x}) - \chi^* \hat{A}_1 \hat{A}_2 + \frac{i v_0^2}{2\omega_0}\nabla^2 \hat{A}_0 + \sqrt{2\gamma_0}\hat{A}_0^{in}\,, \\
\frac{\partial \hat{A}_1}{\partial t} &= -\tilde{\gamma}_1 \hat{A}_1 + \chi \hat{A}_0 \hat{A}_2^\dagger + \frac{i v_1^2}{2\omega_1}\nabla^2 \hat{A}_1 + \sqrt{2\gamma_1}\hat{A}_1^{in}\,, \\
\frac{\partial \hat{A}_2}{\partial t} &= -\tilde{\gamma}_2 \hat{A}_2 + \chi \hat{A}_0 \hat{A}_1^\dagger + \frac{i v_2^2}{2\omega_2}\nabla^2 \hat{A}_2 + \sqrt{2\gamma_2}\hat{A}_2^{in}\,.
\end{aligned} \tag{A1}$$

Here we use a rotating frame such that the three field operators are treated as in a frame rotating with frequency ω_i^0. The relative detuning between the pump laser at $2\omega_L$ and the intracavity pumped mode ω_0 is $\Delta_0 = (\omega_0 - 2\omega_L)/\gamma_0$, and the down-converted modes have relative detunings $\Delta_i = \left(\omega_i - \omega_i^0\right)/\gamma_i$. The terms $\tilde{\gamma}_i = \gamma_i\left(1 + i\Delta_i\right)$ represent the complex cavity decay for each mode, including detunings. However, the quantum Langevin approach has the drawback that it deals with operator equations that are intractable analytically. It was shown in section III that the phase-space that the phase-space representation method generates similar equations, but with a more useful c-number form.

The input-output relations that describe the external modes outside the cavity are [9, 10, 43–45]: $\hat{A}_i^{out} = \sqrt{2\gamma_i}\hat{A}_i - \hat{A}_i^{in}$, where $\hat{A}_i^{in}$ and $\hat{A}_i^{out}$ are the corresponding input and output fields, with input correlations:

$$\begin{aligned}
\left\langle \hat{A}_i^{in}(\boldsymbol{x},t)\hat{A}_j^{in\dagger}(\boldsymbol{x}',t)\right\rangle &= \left(\bar{n}_i^{th}+1\right)\delta_{ij}\delta\left(\boldsymbol{x}-\boldsymbol{x}'\right), \\
\left\langle \hat{A}_i^{in\dagger}(\boldsymbol{x},t)\hat{A}_j^{in}(\boldsymbol{x}',t)\right\rangle &= \bar{n}_i^{th}\delta_{ij}\delta\left(\boldsymbol{x}-\boldsymbol{x}'\right).
\end{aligned} \tag{A2}$$

In our calculations we assume that the reservoirs are in the vacuum state. However, non-zero reservoir temperatures can be readily included. While we do not use these input-output equations here, we note that they are important when dealing with external measurements.

APPENDIX B: POSITIVE-P REPRESENTATION

The positive P-representation generates a genuine (second order) Fokker-Planck equation with positive-definite diffusion, provided the distribution vanishes sufficiently rapidly at the phase-space boundaries. This can then be mapped into a set of c-number Langevin equations similar to the quantum Heisenberg equations, except for additional stochastic terms.

This approach uses a multi-mode coherent state $|\tilde{\boldsymbol{\alpha}}_0, \tilde{\boldsymbol{\alpha}}_1, \tilde{\boldsymbol{\alpha}}_2\rangle \equiv |\tilde{\boldsymbol{\alpha}}\rangle$, defined as an eigenstate of the annihilation operators $\hat{a}_i(\boldsymbol{k})$, where $\tilde{\alpha}_i \equiv \tilde{\alpha}_i(\boldsymbol{k})$ so that the following eigenvalue equation is obtained:

$$\hat{a}_i(\boldsymbol{k})\,|\tilde{\boldsymbol{\alpha}}\rangle = \tilde{\alpha}_i(\boldsymbol{k})\,|\tilde{\boldsymbol{\alpha}}\rangle\,. \tag{C1}$$

The positive-P representation then expands the density matrix in terms of coherent state projection operators [40], which is always possible as a positive distribution:

$$\hat{\rho} = \int d^{6M}\tilde{\boldsymbol{\alpha}} d^{6M}\tilde{\boldsymbol{\alpha}}^+ \frac{|\tilde{\boldsymbol{\alpha}}\rangle\,\langle\tilde{\boldsymbol{\alpha}}^{+*}|}{\langle\tilde{\boldsymbol{\alpha}}^{+*}\,|\tilde{\boldsymbol{\alpha}}\rangle} P\left(\tilde{\boldsymbol{\alpha}}, \tilde{\boldsymbol{\alpha}}^+\right)\,. \tag{C2}$$

In the positive P-representation the coherent amplitudes $\tilde{\alpha}_i(\boldsymbol{k},t)$ satisfy time-dependent stochastic differential equations. It is simplest to write these equations in a form analogous to classical equations by introducing stochastic fields A_i , A_i^+ defined as:

$$A_i(\boldsymbol{x},t) = \frac{1}{L}\sum_{\boldsymbol{k}} e^{i\boldsymbol{k}\cdot\boldsymbol{x}}\tilde{\alpha}_i(\boldsymbol{k},t)\,, \tag{C3}$$

together with a stochastic conjugate A_i^+ which is a c-number, rather than an operator field. It is only conjugate to A_i in the mean: it is stochastically equivalent to the conjugate operator.

1. Noises of the stochastic equations

We note that while our derivation of the set of stochastic equations given in Eq. (3.1) is formally based on the Itô stochastic calculus, in this case either Itô or Stratonovich stochastic calculus gives identical results. These complex noise terms can be constructed from four delta-correlated real Gaussian noise fields $\left(\xi_x, \xi_y, \xi_x^+, \xi_y^+\right)$, with the mapping:

$$\begin{aligned}
\xi_{1,2}(\boldsymbol{x},t) &= \left[\xi_x(\boldsymbol{x},t) \pm i\xi_y(\boldsymbol{x},t)\right]/\sqrt{2}\,, \\
\xi_{1,2}^+(\boldsymbol{x},t) &= \left[\xi_x^+(\boldsymbol{x},t) \pm i\xi_y^+(\boldsymbol{x},t)\right]/\sqrt{2}\,.
\end{aligned} \tag{C4}$$

It follows that the stochastic fields in the positive P-representation for the ξ_1 and ξ_2 fields are complex conjugate, i.e.,

$$\xi_1(\boldsymbol{x},t) = \xi_2^*(\boldsymbol{x},t)\,, \qquad \text{and} \qquad \xi_1^+(\boldsymbol{x},t) = \left(\xi_2^+(\boldsymbol{x},t)\right)^*. \tag{C5}$$

The physics of the noise is that it describes a departure from coherent behavior. The deterministic terms correspond to the evolution of coherent states. However, the true quantum state does not remain coherent. Instead it develops, via the noise terms, into squeezed, entangled,

and even more complex states. Despite this complexity, there are simple, universal properties caused by these noise terms at the critical point.

We note that there are no 'normal' noise correlations, that is, $\left\langle \xi_i(\boldsymbol{x},t)\xi_k^+(\boldsymbol{x}',t')\right\rangle = 0$. This is due to our assumption that the optical reservoirs are at zero temperature, which is an excellent approximation at optical frequencies. If there are thermal reservoirs, as can occur in microwave devices, then additional reservoir correlations must be included, which are proportional to the thermal occupation number. More generally, our model includes only the minimal noise due to fundamental quantum effects, but there can be a range of additional technical noise sources in practical devices, caused by temperature fluctuations, laser intensity fluctuations and laser phase noise [7, 69].

Funding

Australian Research Council (ARC); Conselho Nacional de Desenvolvimento Científico e Tecnológico (CNPq).

[1] C. Bolman and A. C. Newell, "Natural patterns and wavelets," Rev. Mod. Phys. **70**, 289 (1998); J. P. Gollub and J. S. Langer, "Pattern formation in nonequilibrium physics," Rev. Mod. Phys. **71**, S396 (1999).

[2] M. C. Cross and P. C. Hohenberg, "Pattern formation outside of equilibrium," Rev. Mod. Phys. **65**, 851 (1993); P. C. Hohenberg and B. I. Halperin, "Theory of dynamic critical phenomena," Rev. Mod. Phys. **49**, 435 (1977).

[3] J. Swift and P. C. Hohenberg, "Hydrodynamic fluctuations at the convective instability," Phys. Rev. A **15**, 319 (1977).

[4] R. Graham and H. Haken, "Laserlight -First example of a second order phase transition far from thermal equilibrium," Z. Physik **237**, 31 (1970); V. deGiorgio and M. O. Scully, "Analogy between the Laser Threshold Region and a Second-Order Phase Transition," Phys. Rev. A **2**, 1170 (1970).

[5] M. D. Reid, "Demonstration of the Einstein-Podolsky-Rosen paradox using nondegenerate parametric amplification," Phys. Rev. A **40**, 913 (1989); M. D. Reid and P. D. Drummond, "Quantum Correlations of Phase in Nondegenerate Parametric Oscillation," Phys. Rev. Lett. **60**, 2731 (1988); M. D. Reid, P. D. Drummond, W. P. Bowen, E. G. Cavalcanti, P. K. Lam, H. A. Bachor, U. L. Andersen and G. Leuchs, "The Einstein-Podolsky-Rosen paradox: From concepts to applications," Rev. Mod. Phys. **81**, 1727 (2009).

[6] Z. Y. Ou, S. F. Pereira, H. J. Kimble and K. C. Peng, "Realization of the Einstein-Podolsky-Rosen paradox for continuous variables ," Phys. Rev. Lett. **68**, 3663 (1992).

[7] M. D. Reid and P. D. Drummond, "Correlations in nondegenerate parametric oscillation: Squeezing in the presence of phase diffusion," Phys. Rev. A **40**, 4493 (1989).

[8] P. D. Drummond and M. D. Reid, "Correlations in nondegenerate parametric oscillation. II. Below threshold results," Phys. Rev. A **41**, 3930 (1990).

[9] M. J. Collett and C. W. Gardiner "Squeezing of intracavity and traveling-wave light fields produced in parametric amplification", Phys. Rev. A **30**, 1386 (1984); C. W. Gardiner and M. J. Collett, "Input and output in damped quantum systems: Quantum stochastic differential equations and the master equation," Phys. Rev. A **31**, 3761 (1985).

[10] B. Yurke, "Squeezed-coherent-state generation via four-wave mixers and detection via homodyne detectors," Phys. Rev. A **32**, 300 (1985).

[11] L. A. Wu, H. J. Kimble, J. L. Hall and H. Wu, "Generation of Squeezed States by Parametric Down Conversion," Phys. Rev. Lett. **57**, 2520 (1986).

[12] S. Feng and O. Pfister "Stable nondegenerate optical parametric oscillation at degenerate frequencies in Na:KTP,", J. Opt. B **5,** 262–267 (2003).

[13] A. S. Villar, K. N. Cassemiro, K. Dechoum, A. Z. Khoury, M. Martinelli and P. Nussenzveig, "Entanglement in the above-threshold optical parametric oscillator ," J. Opt. Soc. Am. B **24**, 249 (2007).

[14] J. Laurat, T. Coudreau and C. Fabre, in *Quantum Information with continuous variables of atoms and light*, edited by Ed. N. J. Cerf, G. Leuchs and E. S. Polzik (World Scientific Publishing 2007).

[15] J. Laurat, T. Coudreau, G. Keller, N. Treps and C. Fabre, "Effects of mode coupling on the generation of quadrature Einstein-Podolsky-Rosen entanglement in a type-II optical parametric oscillator below threshold ," Phys. Rev. A **71**, 022313 (2005).

[16] J. Laurat, L. Longchambon, C. Fabre and T. Coudreau, "Experimental investigation of amplitude and phase quantum correlations in a type II optical parametric oscillator above threshold: from nondegenerate to degenerate operation," Optics Letters **30**, 1177 (2005).

[17] G. Keller, V. D'Auria, N. Treps, T. Coudreau, J. Laurat and C. Fabre, "Experimental demonstration of frequency-degenerate bright EPR beams with a self-phase-locked OPO," Optics Express **16**, 9351 (2008).

[18] V. D'Auria, A. Chiummo, M. De Laurentis, A. Porzio, S. Solimeno and M. G. A. Paris, "Tomographic characterization of OPO sources close to threshold," Optics Express **13**, 948 (2005); V. D'Auria, C. de Lisio, A. Porzio, S. Solimeno, J. Anwar, and M. G. A. Paris, "Non-Gaussian states produced by close-to-threshold optical parametric oscillators: Role of classical and quantum fluctuations," Phys. Rev. A **81**, 033846 (2010).

[19] G.-L. Oppo, M. Brambilla and L. A. Lugiato, "Formation and evolution of roll patterns in optical parametric oscillators," Phys. Rev. A **49**, 2028 (1994).

[20] E. M. Lifshitz and L. P. Pitaevskii, *Physical Kinetics*, Volume 10 of Course of Theoretical Physics, (Pergamon Press, Oxford 1981).

[21] A. Michelson, "Phase diagrams near the Lifshitz point. I. Uniaxial magnetization," Phys. Rev. B **16**, 577 (1977).

[22] R. M. Hornreich, R. Liebmann, H.G. Schuster and W. Selke, "Lifshitz points in ising systems," Z. Phys. B **35,**

91(1979); R. M. Hornreich, "The Lifshitz point: Phase diagrams and critical behavior," Journal of Magnetic Materials **15,** 387 (1980).

[23] P. D. Drummond and K. Dechoum, "Universality of Quantum Critical Dynamics in a Planar Optical Parametric Oscillator," Phys. Rev. Lett. **95**, 083601 (2005).

[24] V. J. Sánchez-Morcillo, E. Roldán, G. J. de Valcárcel and K. Staliunas, "Generalized complex Swift-Hohenberg equation for optical parametric oscillators," Phys. Rev. A **56**, 3237 (1997).

[25] M. Vaupel, A. Maitre and C. Fabre, "Observation of Pattern Formation in Optical Parametric Oscillators," Phys. Rev. Lett. **83**, 5278 (1999); M. Martinelli, N. Treps, S. Ducci, S. Gigan, A. Maitre and C. Fabre, "Experimental study of the spatial distribution of quantum correlations in a confocal optical parametric oscillator," Phys. Rev. A **67**, 023808 (2003).

[26] S. Ducci, N. Treps, A. Maître and C. Fabre, "Pattern formation in optical parametric oscillators," Phys. Rev. A **64**, 023803 (2001).

[27] J. Lega, J. V. Moloney and A. C. Newell, "Swift-Hohenberg Equation for Lasers," Phys. Rev. Lett. **73**, 2978 (1994).

[28] R. M. Hornreich, M. Luban and S. Shtrikman, "Critical Behavior at the Onset of $\vec{k}$-Space Instability on the λ Line" Phys. Rev. Lett. **35**, 1678 (1975).

[29] E. K. Riedel and F. J. Wegner, "Tricritical exponents and scaling fields" Phys. Rev. Lett. **29**, 349 (1972); P. M. Chaikin and T. C. Lubensky, P*rinciples of Condensed Matter Physics* (Cambridge University Press 1995); A. Bonanno and D. Zappalà, Nuclear Physics B **893**, 501 (2015).

[30] K. Staliunas, "Laser Ginzburg-Landau equation and laser hydrodynamics," Phys. Rev. A **48**, 1573 (1993). P. C. Hohenberg and A. P. Krekhov, "An introduction to the Ginzburg–Landau theory of phase transitions and nonequilibrium patterns," Physics Reports **572**, 1 (2015).

[31] A. Gatti and L. Lugiato, "Quantum images and critical fluctuations in the optical parametric oscillator below threshold," Phys. Rev. A **52**, 1675 (1995); A. Gatti, H. Wiedemann, L. A. Lugiato, I. Marzoli, G.-L. Oppo and S. M. Barnett, "Langevin treatment of quantum fluctuations and optical patterns in optical parametric oscillators below threshold," Phys. Rev. A **56**, 877 (1997); A. Gatti, L.A. Lugiato, G.-L. Oppo, R. Martin, P. Di Trapani and A. Berzanskis, "From quantum to classical images," Opt. Express **1**, 21 (1997); L. A. Lugiato, A. Gatti and E. Brambilla, "Quantum imaging," J. Opt. B **4**, S176 (2002).

[32] P. D. Drummond, K. J. McNeil and D. F. Walls, "Non-equilibrium Transitions in Sub/Second Harmonic Generation," Optica Acta **27**, 321 (1980); P. D. Drummond, K. J. McNeil and D. F. Walls, "Non-equilibrium Transitions in Sub/second Harmonic Generation," Optica Acta **28**, 211 (1981).

[33] M. A. M. Marte, H. Ritsch, K. Petsas, A. Gatti, L. Lugiato, C. Fabre and D. Leduc, "Spatial patterns in optical parametric oscillators with spherical mirrors: classical and quantum effects," Optics Express **3**, 71 (1998).

[34] N. Treps, N. Grosse, W. P. Bowen, C. Fabre, H. A. Bachor and P. K. Lam, "A Quantum Laser Pointer," Science **301**, 940 (2003).

[35] C. J. Mertens, T. A. B. Kennedy and S. Swain, "Many body theory of quantum noise," Phys. Rev. Lett. **71**, 2014 (1993).

[36] V. L. Berezinskii, "Destruction of Long-range Order in One-dimensional and Two-dimensional Systems Possessing a Continuous Symmetry Group. II. Quantum Systems," Sov. Phys. JETP **34**, 610 (1972).

[37] J. M. Kosterlitz and D. J. Thouless, "Ordering, metastability and phase transitions in two-dimensional systems," J. Phys. C **6**, 1181, (1973).

[38] S. Chaturvedi, K. Dechoum and P. D. Drummond, "Limits to squeezing in the degenerate optical parametric oscillator," Phys. Rev. A **65**, 033805 (2002); K. Dechoum, P. D. Drummond, S. Chaturvedi and M. D. Reid, "Critical fluctuations and entanglement in the nondegenerate parametric oscillator," Phys. Rev. A **70**, 053807 (2004).

[39] N. D. Mermin and H. Wagner, "Absence of Ferromagnetism or Antiferromagnetism in One- or Two-Dimensional Isotropic Heisenberg Models," Phys. Rev. Lett. **17**, 1133 (1966).

[40] P. D. Drummond and C. W. Gardiner, "Generalised P-representations in quantum optics," J. Phys. A **13**, 2353 (1980).

[41] H. Haken, *Laser Theory*, (Springer Berlin Heidelberg 1984).

[42] C. Lamprecht, M. K. Olsen, P. D. Drummond and H. Ritsch, "Positive-P and Wigner representations for quantum-optical systems with nonorthogonal modes," Phys. Rev. A **65**, 053813 (2002).

[43] C. W. Gardiner and P. Zoller, *Quantum Noise* (Springer, Berlin 2000).

[44] B. Yurke in *Quantum Squeezing*, edited by P. D. Drummond and Z. Ficek (Springer, Berlin, 2004); D. F. Walls G. J Milburn, *Quantum Optics* (Springer, Berlin, 2008)

[45] P. D. Drummond and M. Hillery, *The Quantum Theory of Nonlinear Optics* (Cambridge University Press 2014).

[46] I. Carusotto and C. Ciuti, "Quantum fluids of light," Rev. Mod. Phys. **85**, 299 (2013).

[47] M. Hillery and L. D. Mlodinow, "Quantization of electrodynamics in nonlinear dielectric media," Phys. Rev. A **30**, 1860 (1984).

[48] H. J. Carmichael, *Statistical Methods in Quantum Optics 1* (Springer, Berlin 2002).

[49] E. Wigner, "On the Quantum Correction For Thermodynamic Equilibrium," Phys. Rev. **40**, 749 (1932).

[50] P. D. Drummond, "Fundamentals of higher order stochastic equations," J. Phys. A **47**, 335001 (2014).

[51] K. Husimi, "Some Formal Properties of the Density Matrix," Proc. Phys. Math. Soc. Japan **22**, 264 (1940).

[52] R. Zambrini, S. M. Barnett, P. Colet and M. San Miguel, "Non-classical behavior in multimode and disordered transverse structures in OPO. Use of the Q-representation," Eur. Phys. J. D **22**, 461 (2003).

[53] R. J. Glauber, "Coherent and Incoherent States of the Radiation Field," Phys. Rev. **131**, 2766 (1963); E. C. G. Sudarshan, "Equivalence of Semiclassical and Quantum Mechanical Descriptions of Statistical Light Beams," Phys. Rev. Lett. **10**, 277 (1963).

[54] M. Santagiustina, E. Hernandez-Garcia, M. San-Miguel, A. J. Scroggie and G.-L. Oppo, "Polarization patterns and vectorial defects in type-II optical parametric oscillators," Phys. Rev. E, **65**, 036610 (2002).

[55] R. Zambrini, A. Gatti, L. Lugiato and M. San Miguel, "Polarization quantum properties in a type-II optical

parametric oscillator below threshold," Phys. Rev A **68**, 063809 (2003).

[56] G. Izús, M. San Miguel and D. Walgraef, "Polarization coupling and pattern selection in a type-II optical parametric oscillator," Phys. Rev. E **66**, 36228 (2002).

[57] S. Longhi, "Alternating rolls in non-degenerate optical parametric oscillators," J. Mod. Opt, **43**, 1569 (1996); G. J. de Valcárcel and E. Roldán and K. Staliunas, "Cavity solitons in nondegenerate optical parametric oscillation," Opt. Commun. **181**, 207 (2000); K. Staliunas, "Transverse Pattern Formation in Optical Parametric Oscillators," J. Mod. Opt. **42**, 1261 (1995); G.-L. Oppo, M. Brambilla, D. Camesasca, A. Gatti and L. A. Lugiato, "Spatiotemporal Dynamics of Optical Parametric Oscillators," J. Mod. Opt. **41**, 1151 (1994); S. Longhi, "Spatial solitary waves in nondegenerate optical parametric oscillators near an inverted bifurcation," Opt. Commun. **149**, 335 (1998); S. Longhi and A. Geraci, "Swift-Hohenberg equation for optical parametric oscillators," Phys. Rev. A **54**, 4581 (1996).

[58] E. M. Lifshitz and L. P. Pitaevskii, *Statistical Physics, Part 2*, in Volume 9 of the Course of Theoretical Physics, (Pergamon Press, Oxford 1980).

[59] P. D. Drummond and I. K. Mortimer, "Computer simulations of multiplicative stochastic differential equations," J. Comp. Phys. **93**, 144 (1991); M. J. Werner and P. D. Drummond, "Robust Algorithms for Solving Stochastic Partial Differential Equations," J. Comp. Phys. **132**, 312 (1997).

[60] G. R. Collecutt and P. D. Drummond, "Xmds: eXtensible multi-dimensional simulator," Comput. Phys. Commun. **142**, 219 (2001); S. Kiesewetter, R. Polkinghorne, B. Opanchuk and P. D. Drummond,"xSPDE: extensible software for stochastic equations", SoftwareX in press.

[61] G. Kozyreff and M. Tlidi, "Nonvariational real Swift-Hohenberg equation for biological, chemical, and optical systems," Chaos **17**, 037103 (2007); M. Tlidi, Paul Mandel and R. Lefever "Localized structures and localized patterns in optical bistability," Phys. Rev. Lett. **73**, 640 (1994).

[62] J. Yin and D. P. Landau, "Phase diagram and critical behavior of the square-lattice Ising model with competing nearest-neighbor and next-nearest-neighbor interactions," Phys. Rev. E **80**, 051117 (2009).

[63] Shang-Keng Ma, *Modern theory of critical phenomena*, (W. A. Benjamin, Reading, Massachusetts 1976); P. Kopietz, L. Bartosch and F. Schtz, *Introduction to the Functional Renormalization Group* (Springer, Berlin, 2010).

[64] K. Staliunas, "Spatial and temporal noise spectra of spatially extended systems with order disorder phase transitions," Int. Journal of Bifurcation and Chaos **11**, 2845 (2001); K. Staliunas, "Spatial and temporal spectra of noise driven stripe patterns," Phys. Rev. E **64**, 066129 (2001).

[65] K. Staliunas and M. Tlidi, "Hyperbolic Transverse Patterns in Nonlinear Optical Resonators," Phys. Rev. Lett. **94**, 133902 (2005).

[66] K. Staliunas, G. Slekys and C. O. Weiss, "Nonlinear Pattern Formation in Active Optical Systems: Shocks, Domains of Tilted Waves, and Cross-Roll Patterns," Phys. Rev. Lett. **79**, 2658 (1997).

[67] K. Staliunas and V. J. Sanchez-Morcillo, *Transverse Patterns in Nonlinear Optical Resonators*, Springer Tracts Mod. Phys. (Springer-Verlag, Berlin, 2003).

[68] I. S. Gradshteyn and I. M. Ryzhik. *Table of integrals, series, and products (7th ed)*. Academic Press, Amsterdam, (2007).

[69] P. D. Drummond and M. D. Reid, "Laser bandwidth effects on squeezing in intracavity parametric oscillation," Phys. Rev. A **37**, 1806 (1988).